Available online at www.sciencedirect.com

ScienceDirect

Procedia Engineering 133 (2015) 90 – 101

Procedia Engineering

www.elsevier.com/locate/procedia

6th Fatigue Design conference, Fatigue Design 2015

Fatigue of Clip Connectors for Offshore Drilling Risers under the Combined Influence of High Mean Stress and Biaxial Tension

Vidit Gaur[a,b]*, Véronique Doquet[a], Emmanuel Persent[b], Eléonore Roguet[b]

[a] *LMS, Ecole Polytechnique, Université Paris-Saclay UMR CNRS 7649, Palaiseau, France*
[b] *IFP Energies Nouvelles, 1 et 4 avenue de Bois-Préau, 92852 Rueil-Malmaison, France*

Abstract

Push-pull fatigue tests at various R ratios ($\sigma_{min}/\sigma_{max}$), as well as combined cyclic tension and internal pressure tests with various proportions of each loading were run on a 2.5%Cr-1%Mo steel to investigate separately the effects of a mean stress and of positive stress biaxiality. Fatigue lives were found to decrease with increasing mean stress at fixed biaxiality and a non-linear effect of stress biaxiality on fatigue lives was observed at a fixed R ratio. The damage mechanisms were found to change with both parameters and these modifications were analyzed. Many popular multiaxial fatigue criteria were unable to describe all the data. Thus, a new fatigue criterion based on Gerber's parabola, has been proposed that captures the evolution of the endurance limit under the combined effect of mean stress and biaxial tension.

© 2015 Published by Elsevier Ltd. This is an open access article under the CC BY-NC-ND license (http://creativecommons.org/licenses/by-nc-nd/4.0/).
Peer-review under responsibility of CETIM

Keywords: biaxial tension; fatigue criteria; damage mechanisms; fish-eye; intergranular; internal crack initiation

1. Introduction

The steel riser tubes used in deep offshore oil drilling can conveniently and quickly be connected /disconnected using "clip connectors" designed at IFP Energies Nouvelles (IFPEN). The riser assembly experiences sea waves-induced cyclic bending and thus, potential fatigue damage. Two situations are encountered: the connected mode (riser tubes in tension, fixed at top and bottom), with high mean stress ($R = 0.7$) and low amplitude, constituting

* Vidit Gaur. Tel.: +33 (0) 1 69 33 57 55; fax: +33 (0) 1 69 33 57 06.
E-mail address: gaur.vidit@gmail.com

1877-7058 © 2015 Published by Elsevier Ltd. This is an open access article under the CC BY-NC-ND license (http://creativecommons.org/licenses/by-nc-nd/4.0/).
Peer-review under responsibility of CETIM
doi:10.1016/j.proeng.2015.12.631

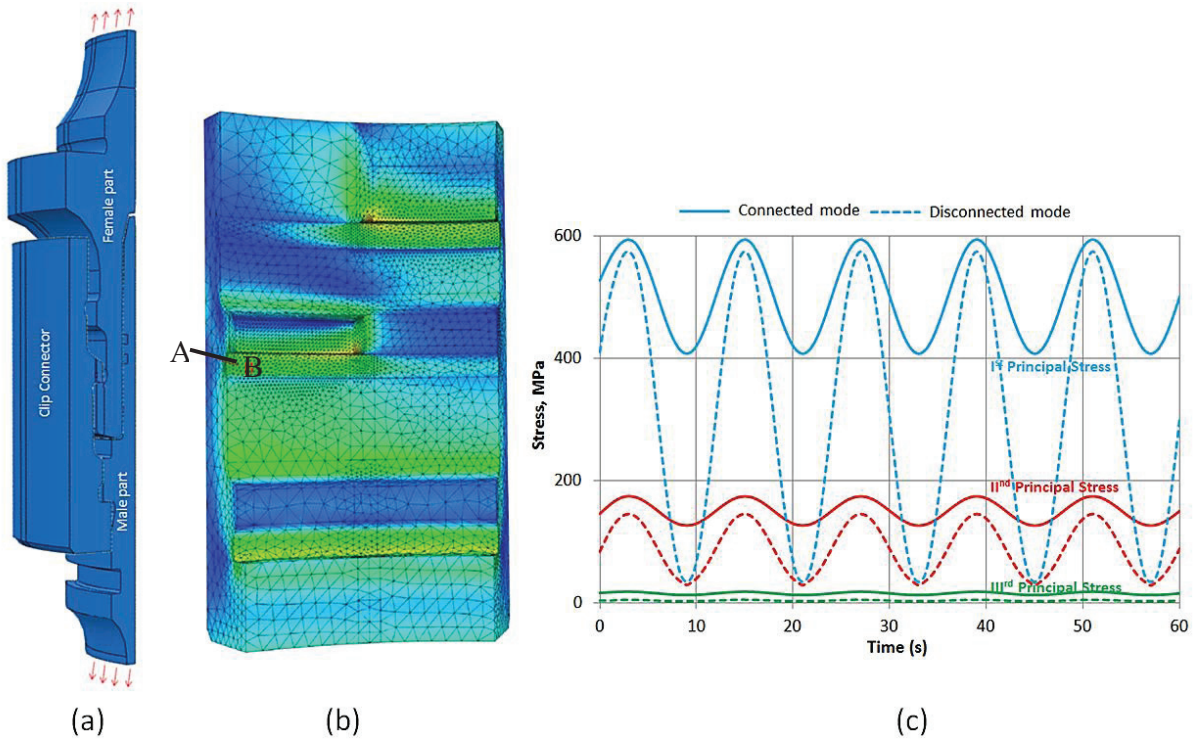

Figure 1 (a) Clip riser FE model. (b) Von-Mises stress contours on clip connector at peak load in connected mode. (c) Computed evolution of three principal stresses in the region below the lugs under connected/disconnected mode.

more than 90% of service life, and the disconnected mode (riser tubes hanging from the top platform), with low mean stress ($R = 0.2$) and high amplitude, constituting less than 10% of service life.

3D elastic-plastic Finite Element (FE) simulations of 50 load cycles representative of connected/disconnected modes showed high stress gradient along thickness (line AB in fig. 1(b)) and in-phase biaxial tension in the critical area of the structure (fig. 1(c)). Both the mean stress effect and the biaxiality effect thus need to be addressed for a proper design of these structures.

Biaxial cyclic tension is frequently encountered in engineering problems concerning for example rotating machines, pressure vessels, or components submitted to thermal fatigue. However, most of the multiaxial fatigue data available in the literature comes from combined tension and torsion tests. The reason for that is twofold. First, high-cycle biaxial tension tests are more challenging in terms of specimen design (cruciform or disc-shaped with a thickness reduction in the central area, or, more simply, tubular) and test analysis (FE and Digital Image Correlation (DIC) measurements are often needed to take stress/strain gradients present in the first two specimens into account) and more demanding in terms of experimental facility (machines with four actuators, or a pressure actuator to bend discs, or tension and pressure actuators, with fluid or gas tightness issues). Second, it is often believed that biaxial tension fatigue is less detrimental than uniaxial fatigue, so that it would not be worth investigating.

However, even though some of the few authors who investigated fatigue or crack growth under such a stress state reported a beneficial effect of biaxial tension [1], some did not observe any effect [2] and some did report a detrimental effect of biaxial tension [3,4]. Some studies [3,5] pointed out that existing fatigue criteria, based on tension-torsion data do not predict correctly the fatigue lives in biaxial tension. In particular the criteria which contain a static hydrostatic stress term cannot discriminate the influence of biaxial tension from that of a mean stress. The purpose of this study is thus to investigate separately those two effects and to model both in a suitable fatigue criterion.

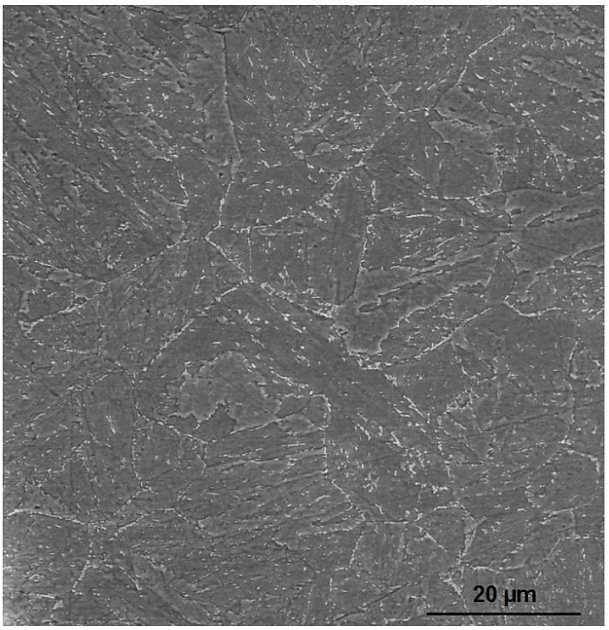

Figure 2 Microstructure of F22 alloy steel

Thus, uniaxial tests were run with various R ratios to investigate mean stress effects while combined tension and internal pressure tests on tubular specimens were run at fixed R ratio with various proportions of each loading mode, to investigate biaxiality effects. The damage mechanisms were analyzed in order to explain the effects observed in terms of fatigue lives. A few reversed torsion tests were also run to determine the corresponding endurance limit, necessary to calibrate several existing fatigue criteria and be able to evaluate their performance in cyclic biaxial tension.

2. Experimental study

2.1. Material and experimental procedures

The clip connector is made of F22 2.5% Cr-1% Mo alloy steel with the measured chemical composition shown in table 1 and basic mechanical properties shown in table 2. The material exhibits a non-textured, tempered martensitic micro-structure with 6.5 µm to 7.7 µm wide equiaxed grains containing remnants of laths (fig. 2). Aluminum-Magnesium-Calcium oxide and manganese sulfide inclusions with an average size of 5 µm are present but do not seem harmful as compared to some less frequent but bigger pores (40-300 µm large) and chemically inhomogeneous areas.

Table 1 Measured chemical composition of F22 alloy steel (weight %).

C	Cr	Mo	O	Mn	Si	Ni	Cu
3.5	2.5	1.1	1.4	0.6	0.2	0.1	0.1

Table 2 Basic mechanical properties of F22 alloy steel.

Proportional limit	0.2% Yield stress	Ultimate tensile stress	Vickers Hardness
600 MPa	694 MPa	780 MPa	267

Cylindrical specimens with surface roughness $R_a < 0.4$ µm were cut from a clip connector and used for stress-controlled push-pull fatigue tests at different R ratios in air at 10 Hz. Specimens of diameter 8 mm for $R \leq 0$, 7 mm for $R = 0.25$ and 6 mm for $R \geq 0.5$ while keeping the same 16 mm gage length, were used. Most of the tests were stopped at 3.10^6 cycles and the corresponding stress amplitude was considered as the endurance limit for that R ratio. However, tests at $R \geq 0.6$ were continued until 10^7 cycles.

Tubular specimens of 25 mm outer diameter, thickness $e = 1$ mm and internal/external surface roughness $R_a < 0.4$ µm were used for in-phase tension and pressure-controlled (internal oil pressure) tests at 10 Hz with $R = 0.25$ on a triaxial testing machine [6]. The axial force amplitude ΔF and pressure amplitude ΔP were chosen so as to get the desired biaxiality ratio (B), defined as:

$$B = \frac{\Delta\sigma_{\theta\theta}}{\Delta\sigma_{zz}} = \frac{\frac{\Delta P\ R_m}{e}}{\frac{\Delta F}{S} + \frac{\Delta P\ R_m}{2e}} \quad (1)$$

Where R_m is the mean radius and 'S' is the cross section of the tubes. Strain gage rosettes were used to check the consistency of expected and measured stress states in the gage length within the elastic regime. The tests were run until a through crack with oil leakage was formed or until specimen ran out at 3.10^6 cycles.

Tubular specimens of 14 mm outer diameter with 0.8 mm thickness, 16mm gage length, and internal/external surface roughness $R_a < 0.4$ µm were used for torque-controlled reversed torsion tests at 10 Hz on the same triaxial testing machine. The tests were stopped at 3.10^6 cycles and the corresponding stress amplitude was considered as the endurance limit.

Scanning Electron Microscopy (SEM) was used to do fractographic observations as well as Energy Dispersive Spectrometry (EDS) chemical micro-analysis. A digital optical microscope was used to perform topographic measurements around crack initiation sites. A dual beam SEM was used for Focused Ion Beam (FIB) sectioning across fish-eye patterns on the fracture surfaces.

X-ray diffraction was used to evaluate the machining residual stresses in the specimens, before and after fatigue testing. More details on that point can be found in [7]. Since, it was concluded that these residual stresses do not control the crack initiation sites, so it will not be reported here.

2.2. Results: Fatigue lives and damage mechanisms

2.2.1. Push-pull fatigue at various R ratios

For uniaxial fatigue tests, both the endurance limit and the slope of the S-N curves drop with increasing R ratio (fig. 3). Endurance limit at different R ratios follow Gerber's parabola [8] (fig. 4). Fatigue criteria with a linear mean normal stress term are thus unlikely to describe these data. At very high mean stresses ($R \geq 0.6$), specimens did not fail at all within 10^7 cycles.

All fatigue failures at $R = -1$, as well as 66% of the failures at $R = -0.5$ and 100% of the failures at $R = 0$ initiated from the surface without any machining or metallurgical defect at the crack initiation site. SEM observation of longitudinal sections of specimens broken at few thousand cycles revealed secondary surface micro-cracks which follow a zig-zag path with frequent deflections along grains or martensite laths boundaries (fig. 5(a)).

By contrast at $R = 0.25$, 88% of the failures initiated from a defect which, when internal (about 40% of those), gave rise to "fish-eye" patterns (fig 5(b)). Some of these defects were pores (fig 5(d)) and some were chemically inhomogeneous material (fig 5(e)-(f)).

Internal cracks propagates without any contact with air, "in vacuum" due to which no oxide layer is formed on crack face thereby making appearance of fish-eye brighter. SEM fractographic observations did not reveal any Optically Dark Area (ODA) [9] or Fine Granular Area (FGA) [10] in the central part of the fish-eyes, but striking differences in the aspect of the fracture surface within and outside it (fig 5(c)). The region within the fish-eye looks much smoother and featureless, with nearly no traces of the underlying microstructure and no striations. The local roughness measured on FIB sections was 0.6 to 1 µm. But, as soon as the crack emerges in air, well-marked

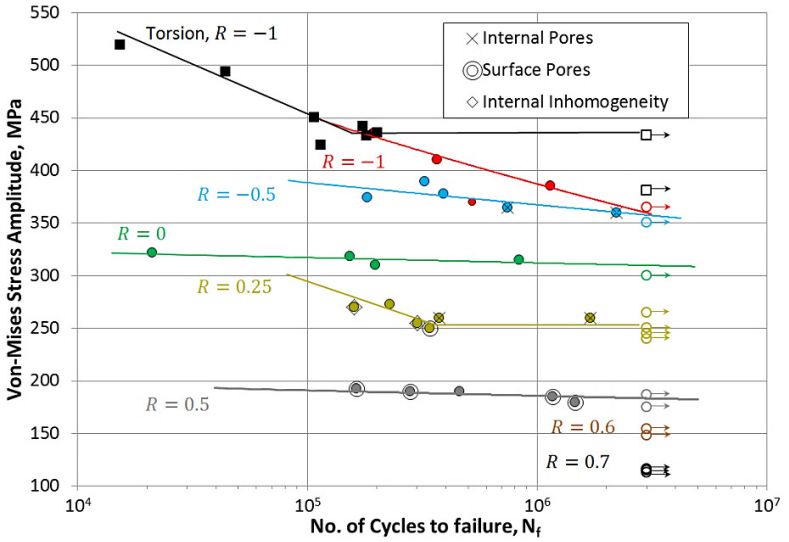

Figure 3 Evolution of fatigue lives with Von-Mises equivalent stress amplitude for torsion test and push-pull fatigue tests at different R ratios. Arrows denote ran out specimens.

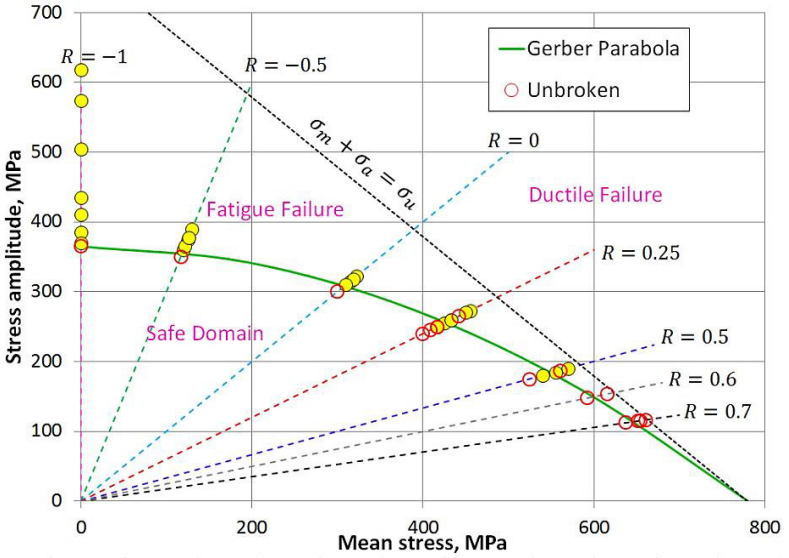

Figure 4 Goodman plot of uniaxial push-pull fatigue data with Gerber's parabola [8].

crystallographic patterns evoking laths as well as a few intergranular facets and many striations could be observed. As a result, the roughness increased to 4 µm.

SEM observations and EDS analyses of fracture surfaces with chemically inhomogeneous areas revealed a crater on one fracture surface and a cluster of matter on the other one, with locally much higher oxygen (30%) and carbon (20%) contents than in the bulk (fig. 5(e)-(f)).

2.2.2. Reversed torsion fatigue

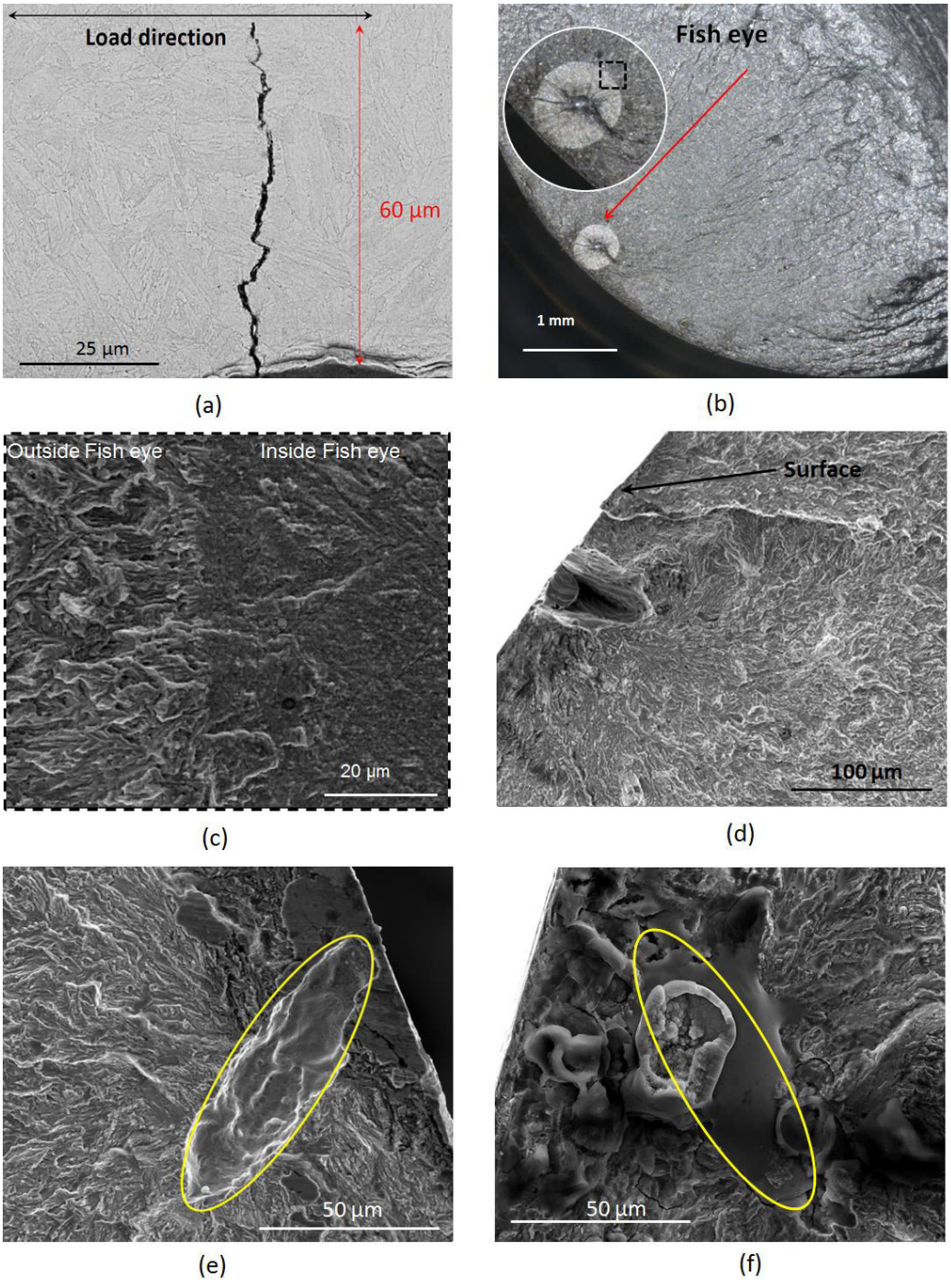

Figure 5 (a) Surface initiated crack at $R = -1$. (b) Defect-induced internal crack initiation with fish-eye at $R = -0.5$. (c) SEM observation at the boundary of the fish-eye shown in (b). (d) Defect induced surface crack initiation at $R = 0.5$. (e) and (f) SEM images of the two halves of a specimen broken due to a crack initiated from a chemical inhomogeneity at $R = 0.25$.

Out of the nine reversed torsion tests, seven gave rise to transverse, shear-mode fatigue failure and two to non-

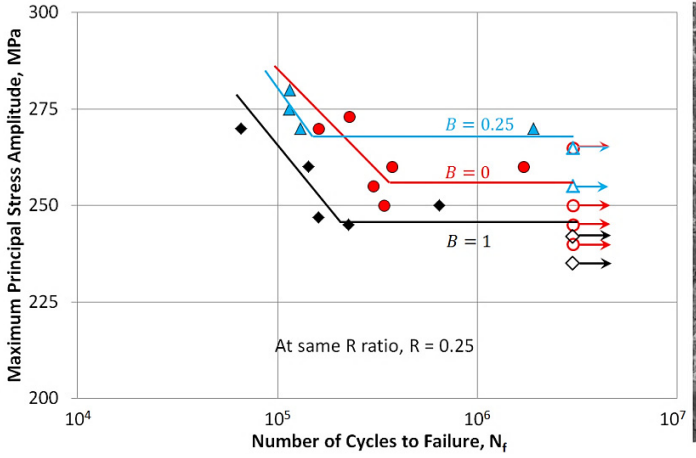

Figure 6 Evolution of fatigue lives under uniaxial and biaxial tension with the maximum principal stress amplitude, for $R = 0.25$.

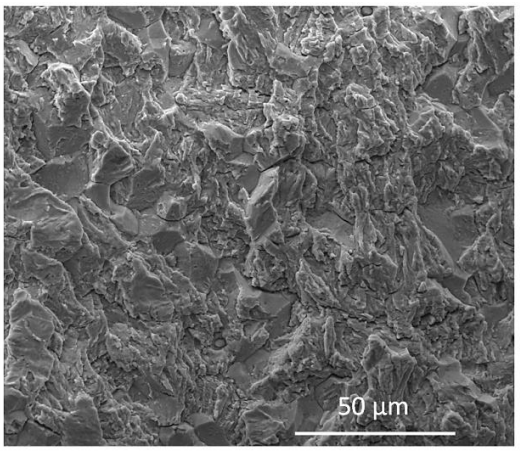

Figure 7 Fracture surface covered with intergranular facets after biaxial tension fatigue at $R = 0.25, B = 1$.

failure. The data allowed an estimation of the endurance limit for torsion (τ_{-1}) at 250 MPa, which was used to calibrate a few fatigue criteria, as discussed below. The fracture surfaces were severely worn and did not provide much information

2.2.3. Biaxial tension fatigue

Fig. 6 compares the evolution of fatigue lives with the amplitude of the maximum principal stress, for different biaxiality ratios. In spite of a large scatter, the asymptote of the Wöhler curve for $B = 0.25$ seems to lie above that for $B = 0$, suggesting a beneficial effect of that specific stress biaxiality, while the contrary seems to hold for $B = 1$. Note that Von-Mises equivalent stress range ($\Delta\sigma_{eq}$) is a non-linear function of load biaxiality (B):

$$\Delta\sigma_{eq} = \Delta\sigma_{zz}\sqrt{1 - B + B^2} \tag{2}$$

It is equal to axial stress range $\Delta\sigma_{zz}$, $0.90\Delta\sigma_{zz}$ and $\Delta\sigma_{zz}$ for $B = 0$, 0.25 and 1, respectively. The seemingly beneficial effect of biaxial tension for $B = 0.25$ might partly be due to a reduction in plastic strain range that would delay crack initiation. Further investigations will be made to support this assumption. However, even though the Von Mises equivalent stress for equibiaxial tension is same as for push-pull, the former has a depreciating effect on fatigue lives. It suggests that Von Mises equivalent stress should be taken into account in a multiaxial fatigue criterion, but that some other terms should also be incorporated to capture this detrimental effect.

All biaxial fatigue failures initiated from the surface. For $B = 0.25$ and thus predominant axial loading, transverse cracks initiated either from the internal or the external surface, while for equibiaxial tension, longitudinal or transverse cracks, initiated always from the internal surface. The latter fact is probably due to the slight gradient in hoop stress, 8% higher on the internal surface than on the external one.

Fractographic observations revealed the presence of a much larger surface fraction of intergranular facets than for uniaxial tests (fig. 7).

3. Discussion

3.1. Crack initiation

Assuming a uniform distribution of defects in the material, the larger the specimen volume (or diameter as gage length is constant), the higher the probability to find a large internal defect. For 7 mm diameter specimens used at $R = 0.25$, this probability was smaller than in the 8 mm diameter specimens used for $R \leq 0$, by a factor of $(7/8)^2$

= 0.76. In spite of this, the proportion of internal cracks was higher at $R = 0.25$, which is thus considered as significant result. For $R = 0.5$ (diameter 6 mm), this probability got further reduced by a factor of $(6/7)^2 = 0.73$ and therefore, the probability of finding the surface defects was increased. This might play a role in the transition from defect-induced internal cracks to defect-induced surface cracks for $R = 0.5$, but there are more intrinsic arguments to explain these transitions, as briefly explained below and more details in [7]. A map of damage mechanisms was thus proposed (fig. 8).

Table 3 Strains and R_σ ratios computed with elastic-plastic constitutive equations at the edge of spherical pore after 100 cycles of representative cyclic loadings on a 3D unit cell finite element model.

R	Δσ (MPa)	Parameters	Internal Pore	Surface Pore
0.25	520	Equivalent plastic strain at first peak	1.8%	2.0%
		Equivalent plastic strain after 100 cycles	2.5%	2.7%
		Tensile strain amplitude after 100 cycles	0.5%	0.5%
		Local R_σ ratio	-1	-0.9
0.5	180	Equivalent plastic strain at first peak	3.6%	4.0%
		Equivalent plastic strain after 100 cycles	3.9%	4.1%
		Tensile strain amplitude after 100 cycles	0.2%	0.2%
		Local R_σ ratio	-0.4	-0.5
0.6	154	Equivalent plastic strain at first peak	3.6% No cyclic plasticity	4% No cyclic plasticity

The analytical solution of Goodier [11] for the stress field around a spherical pore in an infinite elastic medium yields a stress concentration factor (K_t) of 2.04 under uniaxial tension. For the loading conditions corresponding to the endurance limit at $R = 0.25$, 0.5 and 0.6, this is largely sufficient to induce monotonic plastic flow ($2.04\,\sigma_{\max} > \sigma p$) around a pore, as shown by 3D elastic-plastic F.E. simulations on a unit cell model containing $1/8^{th}$ of a pore. The strains and R_σ ratios computed after 100 cycles at the edge of the pore are reported in Table 3.

For $R = 0.25$ and 0.5, cyclic plasticity and ratcheting occur and the steady-state tensile strain ranges are substantial. Based on available fatigue data, the strain amplitude computed for $R = 0.25$ would lead to crack initiation after a few thousand push-pull cycles only, in air. The lack of moist air, the sharp strain gradient on the one hand, and the higher stress triaxiality around an internal pore, on the other hand, would certainly make fatigue crack initiation kinetics different from those in push-pull in air. But, considering the above-mentioned amplitudes, it seems quite improbable that crack initiation from internal pores controls the fatigue lives at $R = 0.25$. The fact that the data points for fatigue failures initiated from internal chemical heterogeneities that produce smaller stress concentrations than internal pores of similar shape do not deviate from the Wöhler curve, mainly corresponding to failures initiated from internal pores, supports the idea that fatigue lives at $R = 0.25$ are indeed controlled by crack growth.

Surface pores lead to higher local strain ranges as compared to internal ones (see Table 3). This might explain why at $R = 0.5$ and thus lower loading ranges, crack initiation from surface defects becomes more frequent than from internal ones.

At $R \geq 0.6$, the stress amplitudes become too small to induce cyclic plasticity around the surface as well as the internal pores, so that crack initiation from the defects seems improbable. Furthermore, even if a crack initiated, it would be unable to grow, as discussed in next section.

The volume of the tubular specimens used for tension and pressure tests at $R = 0.25$ was nearly twice as large as that of the cylindrical specimens used for uniaxial fatigue tests at the same R ratio and so, was the probability to find a large internal defect inside. In spite of this, no internal initiation was observed in biaxial tests. The probable reason could be the stress concentration factor (K_t) which, according to Goodier [11], at spherical pores decreases to 1.87 for biaxial tension with $B = 0.25$ and to 1.36 under equibiaxial loading, instead of 2.04 under uniaxial loading. So, even if they are present, such defects are less prone to initiate cracks under biaxial loading.

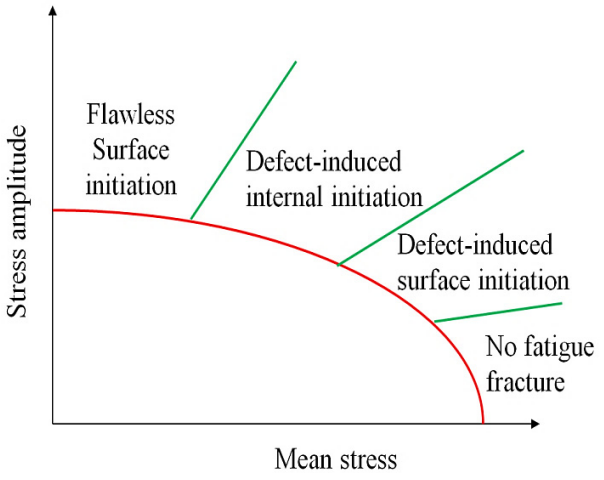

Figure 8 A tentative map of the mechanisms of fatigue failure depending upon the mean stress or R-ratio at 3.10^6 cycles [7].

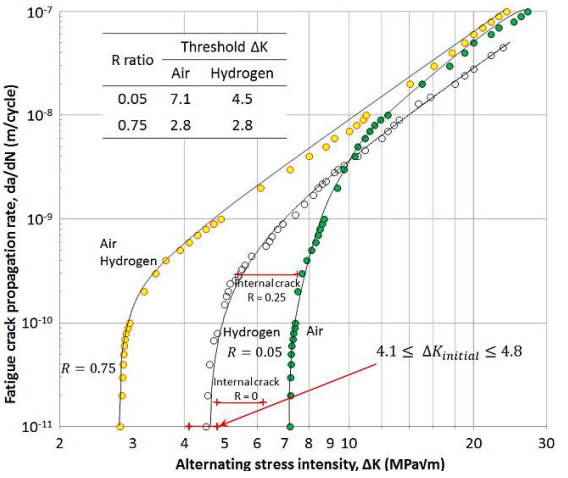

Figure 9 Crack growth kinetics in 2.25Cr-1Mo steel under air and reducing environment (H_2) with some data from present study superimposed (Re-plotted from Suresh et al. [17]).

3.2. Crack growth: Mechanisms and kinetics

3.2.1. Uniaxial fatigue

The absence of fatigue striations inside fish eyes is consistent with the literature on the crack growth in vacuum which attributes it to diffused crack tip plasticity with tip blunting, not as favourable to crack growth as coarse and localized crack tip plasticity in moist air, due to Hydrogen induced localized plasticity [12].The presence of intergranular facets on fatigue fracture surfaces in Ni-Cr-Mo-V and Cr-Mo steels has often been reported as a sign of combined temper and hydrogen embrittlement [13 - 15]. Islam et al. [15] have shown that a preliminary segregation of impurities during the heat treatment is necessary for this phenomenon, but that hydrogen released by a reaction of water vapour with the metal is also necessary. In the present study, the absence of any intergranular or inter-lamellar facet or secondary crack within the fish-eye areas but their presence just outside the fish-eyes is consistent with this conclusion. It is also consistent with the lower roughness within the fish-eye than outside. Roughness-induced closure effects (RICC) are certainly less important during crack growth inside the fish-eyes than outside. In addition oxide-induced closure as well as plasticity-induced closure (PICC) are absent, because of low ΔK, plane strain/stress state for internal cracks and short crack lengths. In summary, internal cracks seem to grow with very few, if any, closure effects, but without any assistance from moist air.

To analyze the crack growth from defects, the major/minor semi-axes: ‘a’ and ‘b’ were measured (considering the defects as elliptical cracks) and the stress intensity factor range (ΔK) at any point along the crack front (designated by its angular position) was calculated, taking into account only the tensile part of the load cycle, as:

$$\Delta K_{I,max} = \Delta\sigma\sqrt{\pi b}/E(k) \tag{3}$$

$$E(k) = \int_0^{\frac{\pi}{2}} \sqrt{1 - \left(1 - \frac{b^2}{a^2}\right)\sin^2\phi}\; d\phi \tag{4}$$

The maximum ΔK occurs at the end of minor axis and is less than 8% different from Murakami’s equation based on √area [16]. Suresh et al.[17] investigated the crack growth kinetics on a similar steel in air and dry hydrogen for $R = 0.05$ and $R = 0.75$. These kinetics have been re-plotted in fig. 9. The crack growth kinetics at $R = 0.75$ can

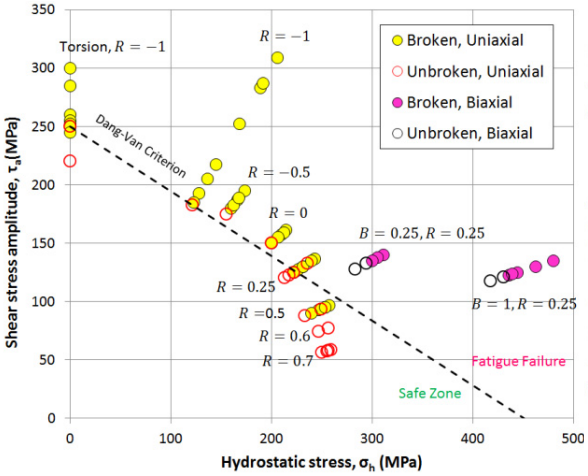

Figure 10 Existing fatigue data plotted against the Dang-Van criterion.

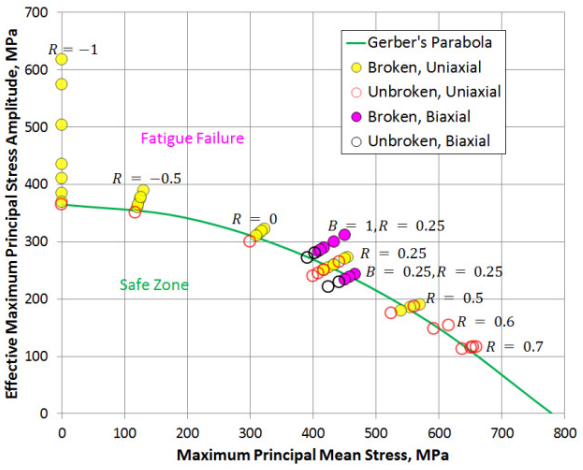

Figure 11 Data from the present study plotted against the new proposed criterion.

probably be considered as closure-free. For all the observed internal cracks, the initial ΔK_I lies between 4.1 and 4.8 MPa√m (see the bar superimposed on fig. 9). In particular, the values found for the two specimens broken at $R = -0.5$ are close to those broken at $R = 0.25$. This is consistent with the idea of Vasudevan et al. [18] that the threshold ΔK for crack growth in vacuum is much less dependent on the R ratio than in air.

Anyway, based on the threshold of 7.1 MPa√m that Suresh et al. [17] obtained in air at $R = 0.05$, and the usually accepted idea that vacuum makes the crack growth slower and the threshold higher, the internal cracks found here at $R = -0.5$ should not propagate. The fact that these cracks actually grow at such a low ΔK in spite of a lower R ratio suggests that the reduction in crack closure compensates the lack of environmental assistance to crack growth

Reloading a ran out specimen from $\sigma_a = 300$ MPa and $R = 0$ to $\sigma_a = 260$ MPa and $R = 0.25$ (failure at 373, 900 cycles) produced a beach mark that indicated the position of the crack front by the end of first loading block and allowed to estimate the mean crack growth rate during the first loading block (1.7×10^{-11} m/cycle while ΔK increased from 4.8 to 6.2 MPa√m at $R = 0$) and the second loading block (2.9×10^{-10} m/cycle while ΔK increased from 5.4 to 7.5 MPa√m at $R = 0.25$). These data (superimposed on fig. 9) corresponding to internal crack growth, fall on the left of the kinetics obtained in air at $R = 0.05$, which also supports the idea that the absence of closure compensates the lack of environmental assistance to crack growth.

For $R = 0.5$, ΔK was estimated to be 3.7 to 3.9 MPa√m for surface defects (fig. 5(d)) which, according to the extensive database of threshold ΔK versus R gathered by Bulloch [19] for tempered martensitic steels, are still compatible with crack growth. By contrast, the ΔK computed for the loading conditions used at $R = 0.6$ or 0.7, assuming the presence of the most critical observed defect in a specimen, comes out to be around 2 MPa√m, which is less than the intrinsic threshold of 2.8 MPa√m found by Suresh et al. [17]. So, even if such defects initiate cracks, they might not be able to propagate. This explains the absence of failure at very high R ratio within 10^7 cycles.

3.2.2. Biaxial tension fatigue

A much larger fraction of intergranular facets on the fracture surfaces of tubular specimens loaded in biaxial tension is perfectly consistent with Ritchie's model for temper and hydrogen-induced embrittlement [20]. Ritchie [20] provided an equation for the related reduction in threshold ΔK due to hydrogen diffusion into the metal which is enhanced by a higher hydrostatic stress. Higher load biaxiality leads to higher hydrostatic stress which enhanced this effect in biaxial tension stress state. Even though an increased fraction of intergranular facets might favour asperity-induced closure, it might also contribute to some detrimental effect of biaxial tension.

3.2.3. Fatigue criteria

Three popular endurance limit criteria have been tested against the data obtained so far: Findley [21], Matake [22] and Dang-Van [23]. Findley's criterion behaves well with uniaxial loading, but is non-conservative for biaxial tension. Matake's criterion is better for biaxial tension, but non-conservative under uniaxial fatigue at $R = 0.5$. Dang-Van's criterion appears non conservative under uniaxial fatigue at $R = 0.5$ and much too conservative for biaxial tension. Fig. 10 shows the plot of existing fatigue data tested against Dang-Van's criterion, given by:

$$a\tau_a + b\sigma_{h,max} \leq \sigma_{-1} \tag{5}$$

Where 'a' and 'b' are material constants, τ_a is the mesoscopic shear stress amplitude, σ_h is hydrostatic stress and σ_{-1} is the fatigue limit under completely reversed push-pull fatigue. All these criteria predict a linear effect of the mean normal or hydrostatic stress, which is not consistent with the fact that uniaxial data follow the Gerber parabola. An alternative criterion, respecting this non-linear dependency, has been proposed as:

$$\frac{\sigma_{\mathrm{eff},a}}{1-\left(\frac{\sigma_{I,m}}{\sigma_u}\right)^2} \leq \sigma_{-1} \tag{6}$$

Where Effective maximum principal stress amplitude, $\sigma_{eff,a}$ is defined as:

$$\sigma_{\mathrm{eff},a} = \sigma_{I,a}\left(\frac{\sigma_{\mathrm{eq},a}}{\sigma_{I,a}}\right)^2\left(\frac{\mathrm{Tr}\,(\sigma_a)}{\sigma_{\mathrm{eq},a}}\right)^x \tag{7}$$

$\sigma_{I,m}$ & $\sigma_{I,a}$ are the maximum principal stress mean & amplitude, $\sigma_{eq,a}$ is Von-Mises equivalent stress amplitude, Tr (σ_a) is trace of stress amplitude, σ_u is ultimate tensile stress and 'x' is the material parameter which for present steel is equal to 1/5. This criterion gets reduced to conventional Gerber's parabola under uniaxial stress conditions. The proposed criterion takes into account the fact that load biaxiality probably delays crack initiation through Von-Mises stress amplitude but favors hydrogen embrittlement though the hydrostatic stress amplitude. Fig. 11 shows that using this criterion, all the data obtained so far can be rationalized.

4. Conclusions

The uniaxial fatigue life of F22 alloy steel as well as the slope of the S-N curves decreases with increasing R ratio. The endurance limit at 3 million cycles follows Gerber's parabola with no fatigue fracture above $R = 0.6$. Surface crack initiation without any defect involved was most often observed for $R = -1, -0.5$ and 0, while an R ratio of 0.25 triggered crack initiation from either surface or internal pores or chemically inhomogeneous areas, leading, in the latter case, to "fish-eye" patterns for relatively low numbers of cycles. A further increase in R ratio to 0.5 promoted defect-initiated surface cracks. Elastic-plastic F.E. computations of the stress/strain fields around internal and surface pores, as well as fracture mechanics arguments rationalized these transitions. Internal cracks seemed to grow without closure effects, which seems to compensate the absence of assistance from moist air, and explain their propagation at a substantially lower ΔK than the threshold measured in air.

The effect of biaxial tension (obtained by combined tension and internal pressure) on fatigue lives seems to be a non-linear function of the biaxiality ratio, B. For $B = 0.25$, the 10% reduction of Von-Mises equivalent stress range compared to uniaxial loading might delay crack initiation and explain the slight improvement of the endurance limit observed. By contrast, equibiaxial cyclic tension seems slightly detrimental, which was attributed to the rise in stress triaxiality, probably responsible for enhanced hydrogen embrittlement, as suggested by the high fraction of intergranular facets.

Neither Dang Van's nor Findley's, nor Matake's criteria described well the endurance limits measured at various mean stresses and biaxialities. An alternative criterion, based on Gerber's parabola, was thus formulated which successfully captured the evolution of endurance limit under combined effect of mean stress and load biaxiality. Tests at different biaxiality ratios and R ratios are still in progress to ensure the validity of the proposed criterion.

References

[1] D. Bellett, F. Morel, A. Morel, and J.L. Lebrun, "A Biaxial fatigue specimen for uniaxial loading," *Strain An Int. J. Exp. Mech.*, vol. 47 (3), pp. 227–240, 2010.

[2] G. Marquis and P. Karjalainen-Roikonen, "Long-life multiaxial fatigue of SG cast iron," *Proc. 6th Int. Conf. Biaxial/Multiaxial Load. Fract.*, pp. 151–159, 2001.

[3] V. Bonnand, J. L. Chaboche, P. Gomez, P. Kanouté, and D. Pacou, "Investigation of multiaxial fatigue in the context of turboengine disc applications," *Int. J. Fatigue*, vol. 33, pp. 1006–1016, 2011.

[4] H. Dietmann, T. Bhonghibhat, and A. Schmid, "Multiaxial fatigue behavior of steels under In-Phase and Out of phase loading including different wave forms and frequencies," *Third Int. Conf. Biaxial/Multiaxial Fatigue, Univ. Stuttgart*, vol. 2, pp. 61.1–61.17, 1989.

[5] I. Koutiri, D. Bellett, F. Morel, L. Augustins, and J. Adrien, "High cycle fatigue damage mechanisms in cast aluminium subject to complex loads," *Int. J. Fatigue*, vol. 47, pp. 44–57, 2013.

[6] V. Doquet and V. De Greef, "Dwell fatigue of a titanium alloy at room temperature under uniaxial or biaxial tension," *Int. J. Fatigue*, vol. 38, pp. 118–129, 2012.

[7] V. Gaur, V. Doquet, E. Persent, C. Mareau, E. Roguet, and J. Kittel, "Surface versus internal fatigue crack initiation in steel: influence of mean stress," *Submitt. to Int. J. Fatigue*, 2015.

[8] W. Z. Gerber, "Calculation of allowable stresses in iron structures," *Z. Bayer Arch. Ing. Ver.*, vol. 6(6), pp. 101–110, 1874.

[9] Y. Murakami, T. Nomoto, and T. Ueda, "On the mechanism of fatigue failure in the super long life regime ($N > 10^7$) cycles. Part II: a fractographic investigation," *Fatigue Fract. Eng. Mater. Struct.*, vol. 23 (11), pp. 903–910, 2000.

[10] K. Shiozawa, Y. Morii, S. Nishino, and L. Lu, "Subsurface crack initiation and propagation mechanism in high-strength steel in a very high cycle fatigue regime," *Int. J. Fatigue*, vol. 28(11), p. 1521-1532, 2006.

[11] J. N. Goodier, "Concentration of Stress Around Spherical and Cylindrical Inclusions and Flaws," *Trans. ASME*, vol. 55 (7), p. 39, 1933.

[12] A. J. McEvily and J. L. Gonzalez Velazquez, "Fatigue Crack Tip Deformation Processes as Influenced by the Environment," *Metall. Trans. A*, vol. 23, pp. 2211–2221, 1992.

[13] S. P. Lynch, "Hydrogen embrittlement (HE) phenomena and mechanisms," in *Stress Corrosion Cracking*, Woodhead Publishing, 2011, pp. 90–130.

[14] H. K. Birnbaum and P. Sofronis, "Hydrogen-enhanced localized plasticity - a mechanism for hydrogen related fracture," *Mater. Sci. Eng. A*, vol. 176, pp. 191–202, 1994.

[15] M. A. Islam, P. Bowen, and J. F. Knott, "Intergranular fracture on fatigue fracture surface of 2.25Cr-1Mo steel at room temperature," *J. Mater. Eng. Perform.*, vol. 14(1), pp. 28–36, 2005.

[16] Y. Murakami, *Metal Fatigue: Effects of small defects and nonmetallic inclusions*. Elsevier Science, 2002.

[17] S. Suresh, G. F. Zamiski, and R. O. Ritchie, "Oxide-induced crack closure: an explanation for near-threshold corrosion fatigue crack growth behavior," *Metall. Trans. A*, vol. 12(8), pp. 1435–1443, 1981.

[18] A. K. Vasudevan, K. Sadananda, and R. L. Holtz, "Analysis of vacuum fatigue crack growth results and its implications," *Int. J. Fatigue*, vol. 27, pp. 1519–1529, 2005.

[19] J. H. Bulloch, "The influence of mean stress or R ratio on the fatigue crack threshold characteristics of steels - A review," *Int. J. Press. Vessel. Pip.*, vol. 47(3), pp. 263–292, 1991.

[20] R. O. Ritchie, "Influence of Impurity segregation on temper embrittlement and on slow fatigue crack growth and threshold behavior in 300-M high strength steel," *Metall. Trans. A*, vol. 8, pp. 1131–1140, 1977.

[21] W. N. Findley, "A theory for the effect of mean stress on fatigue of metals under combined torsion and axial load or bending," *Trans. ASME Ser. B*, vol. 81, pp. 301–306, 1959.

[22] T. Matake, "An explanation of fatigue limit under combined stress," *Bull JSME*, vol. 20, pp. 257–263, 1977.

[23] K. Dang Van, "Sur la résistance a la fatigue des métaux," *These Dr. es Sci. Sci. Tech. l'Armement, 47*, pp. 647–722, 1973.